

# Routine (an)isotropic crystallite size analysis in the double-Voigt approximation done right?

D. Ectors,<sup>a)</sup> F. Goetz-Neunhoeffler, and J. Neubauer

Mineralogy, GeoZentrum Nordbayern, University of Erlangen-Nuernberg (FAU), Erlangen 91054, Bavaria, Germany

(Received 29 August 2016; accepted 4 January 2017)

In this study, the application of (an)isotropic size determination using a recently proposed model for the double-Voigt approach is demonstrated and validated against line profile simulations using the Whole Powder Pattern Modelling approach. The fitting of simulated line profiles demonstrates that the attained crystallite sizes and morphologies are in very reasonable agreement with the simulated values and thus demonstrate that even in routine application scenarios credible size and morphology information can be obtained using the double-Voigt approximation. The aim of this contribution is to provide a comprehensive introduction to the problem, address the practical application of the developed model, and discuss the accuracy of the double-Voigt approach and derived size parameters. Mathematical formulations for the visualization of modeled morphologies, supporting the application of the recently developed macros, are additionally provided. © 2017 International Centre for Diffraction Data. [doi:10.1017/S0885715617000070]

Key words: anisotropic crystallite size, size–strain, Rietveld, double-Voigt, TOPAS

## I. INTRODUCTION

The topic of obtaining accurate crystallite sizes and the average morphology of the coherent scattering domains with size distributions is still a rather controversial topic. After almost a century (Scherrer, 1918) of continuous developments, in technical-oriented studies frequently the “crystallite sizes” are still derived by applying apparently random “Scherrer constants” to measured full-widths at half-maximums (FWHMs). In spite of numerous proofs of the inferiority of such approaches, because of the lack of a direct physical meaning of the derived apparent crystallite sizes (Langford and Wilson, 1978), the popularity is probably given by the apparently easy application and the fact of inclusion of such methods in basic X-ray diffraction textbooks. The derived “sizes” may still be a very rough approximation of the magnitude of “crystallite sizes”; however, very few times the appropriate meaning, especially in case of size distributions (Langford and Wilson, 1978) is stated. The term “crystallite sizes” critically depends on what exact type of “crystallite size” is reported and should always be clearly defined on a physical basis. Also to consider that the derivation of just one moment quotient of a size distribution is a very unreliable measure of the underlying size distribution, as Scardi (2008; Figure 1) stressed.

State-of-the-art methods such as the Whole Powder Pattern Modelling (WPPM) approach (Scardi and Leoni, 2002) and advanced line profile approximations as the double-Voigt approach (Langford, 1980; Balzar and Ledbetter, 1993) for Rietveld refinements, with proven physical backgrounds receive however less attention in practical studies.

An additional “problem” in real samples during powder diffraction experiments is often anisotropic peak broadening owing to the morphology of the coherent scattering domains. The effect of the morphology and size on the line profile is very well established (e.g., Langford and Wilson, 1978). Yet Rietveld compatible approaches are however either based on phenomenological models (Stephens, 1999) originally developed for anisotropic microstrain [Note that the commonly encountered terminology “microstrain/strain” is technically misleading, only the resulting distortions are measurable owing to the introduced order dependent broadening contribution.] broadening or limited in the choice of geometric models (Balić Žunić and Dohrup, 1999) and not very straight forward in the interpretation nor very stable for the application in complex mixtures.

Recently a fully physically sound approach was developed (Ectors *et al.*, 2015a, b) for the double-Voigt approximation, enabling a rapid, stable, and reliable treatment of such effects even in complex cementitious systems and *in situ* experiments (Ectors, 2016; Hurlé *et al.*, 2016).

The following paragraph is intended to provide a comprehensive introduction to the physical background of the measures of “crystallite sizes” in the focus of Rietveld refinements.

## II. CRYSTALLITE SIZES – NUTS AND BOLTS

Assuming a theoretical spherical single crystallite of a defined size (e.g., diameter), the theoretical line profile can easily be calculated. The experimentally observed peaks however will be a convolution of the theoretical line profile and instrumental contributions. Therefore either a line profile standard, typically LaB<sub>6</sub>, is measured to correct for the instrumental contribution or a convolution/fundamental parameter approach (Cheary and Coelho, 1992) is used to deconvolute the physical line profile from the experimental line profile.

<sup>a)</sup> Author to whom correspondence should be addressed. Electronic mail: dominique.ectors@fau.de

Direct deconvolution methods such as the prominent method of Stokes (1948) are less common nowadays since only non-overlapping peaks can be deconvoluted reasonably and an implementation of such methods in Rietveld compatible approaches is not easily possible.

After this fundamental step one can either try to simulate and match the physical line profile, for instance with the *WPPM* method or measure the line profile breadth using different methods. While there is considerable effort to implement the full power of the *WPPM* approach in Rietveld compatible approaches there are however without doubt still situations where physical line profile simulation is not the method of choice, e.g. in complex multiphase refinements with highly overlapping peak contributions. At the moment also the choice of anisotropic geometries in the *WPPM* approach is rather limited and restricted to some high-symmetric crystal systems owing to the complex nature of the CVFs (common volume functions) required for the simulation of accurate physical line profiles. To note that discrete geometries can however be considered numerically by the proposed algorithm of Leonardi *et al.* (2012).

The later “measurement” methods have a long history of application in line profile analysis. The most commonly derived are the measure of the integral breadth (von Laue, 1936) and the variance (slope) (Tournarie, 1956a, b; Wilson, 1962a) equivalent to the Fourier (Bertaut, 1949a, b) derived “size”. The attained values, the so-called apparent crystallite sizes of such measurements, have direct physical meanings and in most cases differ from each other. The apparent crystallite size  $\varepsilon_\beta$  derived from the measure of the integral breadth represents a volume-averaged mean thickness through the crystallite measured parallel to the scattering vector  $hkl$ . On the other hand, the apparent crystallite size  $\varepsilon_K$  from the measure of the variance slope (or from the Fourier method) represents a surface or area averaged mean thickness through the crystallite measured parallel to the scattering vector  $hkl$  (e.g., Langford and Wilson, 1978). These two measures are thus directly connected to a size parameter of the crystallite. Both measures can be related to the diameter of the crystallite  $D = 4/3 * \varepsilon_\beta$  or  $D = 3/2 * \varepsilon_K$ . The situation changes when considering a size distribution of spherical crystallites. Then still the relations hold  $\langle D_V \rangle = 4/3 * \varepsilon_\beta$  and  $\langle D_A \rangle = 3/2 * \varepsilon_K$  (e.g., Langford *et al.*, 2000) but  $\langle D_V \rangle$  is the so-called volume-weighted diameter and  $\langle D_A \rangle$  is the so-called area (or surface)-weighted diameter. Those two diameters represent different moment quotients of the diameter distribution (thus produce different diameters or size parameters) and can be used to derive the later distributions if a certain distribution function type is assumed (e.g., the frequently observed or imposed log-normal distribution, Langford *et al.*, 2000).

So far, only spherical crystallites are discussed here. The complexity rises by considering a large fraction of the crystallites to follow a certain morphology (e.g., an ellipsoid, a cylinder, or a cuboid). Numerous examples can be found concerning so-called nanorods, nanocubes, etc. in the nanoparticle area. Very often the orientation of such morphology is in equilibrium with the symmetry of the crystal system.

If the crystallites exhibit a certain morphology other than a sphere and a non-random orientation in the reciprocal lattice, then the apparent crystallite sizes  $\varepsilon_\beta$  and  $\varepsilon_K$  will be dependent on the  $hkl$  (or more specific be a function of  $hkl$ ) of the respective Bragg peak since as stated earlier the average thicknesses

are measured parallel to the scattering vector and will be different for each “direction” of view. This will effectively produce different breadths (and different physical line profiles) in dependence of  $hkl$ , known as anisotropic (size) peak broadening. Indeed powder diffraction using the Bragg peaks as information is the only non-imaging technique to provide such directional size information in contrast to small angle scattering and PDF (pair distribution function) techniques. A more detailed yet comprehensive discussion on the apparent crystallite sizes and influences on the physical line profile is available, e.g. in Wilson [1962b; chapter IV].

The basic mechanism of the here discussed previously developed model (Ectors *et al.*, 2015a, b) is to calculate on the fly both  $\varepsilon_K$  and  $\varepsilon_\beta$  in dependence of the main radii  $r_x$ ,  $r_y$ , and  $r_z$  of geometric shapes (Figure 1) in reference to spherical coordinates. The corresponding spherical coordinate system is then oriented in the reciprocal crystal system by defining two orthogonal reciprocal vectors  $hkl$ . In this way, all common crystal systems can be treated with the exact same approach. Once the orthogonal coordinate system of the geometric shape is properly oriented, the corresponding apparent crystallite sizes for each  $hkl$  are calculated constrained to the chosen geometrical shape and orientation.

The respective apparent crystallite sizes can then be used to directly calculate corresponding parameters of the size-Voigt-approximation (Ectors *et al.*, 2015b). In this context, it is important to stress the important benefit of the double-Voigt approach allowing separate treatment of size and strain by two individual Voigt functions and the possibility to evaluate both the respective volume- and area-weighted apparent crystallite sizes simultaneously. Commonly available integral breadth methods require a combination with Fourier methods to measure both volume- and area-weighted apparent sizes and therefore depend critically on the accuracy of the two individual methods.

The previously developed model was implemented in the *TOPAS* (Bruker AXS Inc., Madison, WI, USA) Rietveld environment as an automated macro and is available free of charge in the supplemental material of Ectors *et al.* (2015b) (see *TOPAS* macros file).

The next paragraph is intended to give practical advice how to properly parameterize and orient the geometric models in different crystal systems.

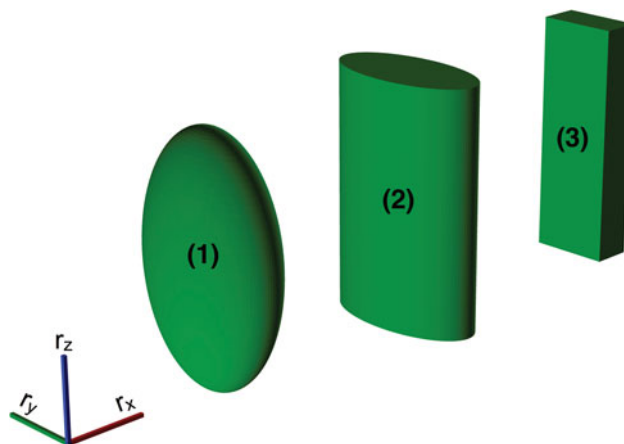


Figure 1. (Color online) Geometric models (1) triaxial ellipsoid (2) elliptic cylinder (3) cuboid currently implemented in the *AnisoCS* and *AnisoCSg* macro with indicated directions of the main radii  $r_x$ ,  $r_y$ , and  $r_z$  (figure created with *OpenSCAD* available at <http://www.openscad.org>).

### III. APPLICATION OF THE MODEL IN THE TOPAS ENVIRONMENT

The former macro is most conveniently stored in the *local.inc* file of the *TOPAS* environment. The framework consists of two refinement macros (*AnisoCS* and *AnisoCSg*) and two optional output macros. *AnisoCS* is the fundamental macro to call instead of the built-in macros for the isotropic size treatment (*CS\_L*, *CS\_G*, or *LVol\_FWHM\_CS\_G\_L*). *AnisoCS* calculates the area- or surface-weighted apparent crystallite sizes for each *hkl* of a structure (*str*) or the so-called *hkl-phase* in dependence of the chosen geometric model and refineable main radii in respect to the chosen orientation in the reciprocal lattice of a phase. For each *hkl* thus the Lorentzian integral breadth is strictly coupled to the refinement parameters. The additional *AnisoCSg* macro adds the Gaussian component to the Voigt size function in dependence of a refineable distribution parameter  $\tau$  (see Ectors *et al.*, 2015b for more details).

Since the Lorentzian part of the Voigt function always dominates the size broadening (Balzar and Ledbetter, 1993), this order is meaningful. Indeed for practical application the consideration of the Lorentzian part only is frequently sufficient to dramatically improve the fit in case of anisotropic (size) broadening.

The correct input parameters for the macro are of huge importance for physical sound results. Therefore, the meaning of the respective refinement parameters will be discussed in detail.

The *AnisoCS* macro is for example called by:

*AnisoCS*(1, 0, 0, 1, 1, 0, 0, rx, 5, ry, 10, rz, 15, !pc, 0, !tc, 0, !nc, 0, 0).

The first number “*AnisoCS*(1”, is the choice of geometric model; **1** for an triaxial ellipsoid; **2** for an elliptic cylinder; **3** for a cuboid (rectangular parallelepiped). One should first consider a symmetry following model.

The following vector “*AnisoCS*(1, **0, 0, 1**,” is the *hkl* vector of the **Z**-axis of the geometric model here (**001**). The **Z**-axis is also the special direction for the flat face of the cylinder model. The following vector “*AnisoCS*(1, 0, 0, 1, **1, 0, 0**,” is *hkl* vector of the **X**-axis of the geometric model here (**100**). One has to make sure that both vectors are orthogonal to each other since the considered geometric models are orthogonal.

“*AnisoCS*(1, 0, 0, 1, 1, 0, 0, **rx, 5, ry, 10, rz, 15**,” are the variable names and initial values of the corresponding refineable main radii of the models. The parameter names can be freely chosen or coupled like for example “rx, 5, rx, 5, rz, 15”, in order to restrict the model here to a biaxial ellipsoid. Constraints can be applied in the normal *TOPAS* notation, e.g. “rx, 5 min=1; max=10.” One should again consider the symmetry of the crystal system.

“*AnisoCS*(1, 0, 0, 1, 1, 0, 0, rx, 5, ry, 10, rz, 15, **!pc, 0, !tc, 0, !nc, 0, 0**” are the variable names and values of additional rotation of the model and the last “**0**”) is an orientation help in triclinic systems. These parameters and values should in conventional refinements *not be modified or refined* without the full awareness of the symmetry and possible cross-correlations (see Ectors *et al.*, 2015a for details).

In summary, for routine application one should decide or test [In order to truly be able to differentiate between ellipsoids, cylinders, and cuboids a good statistic of independent observation directions (*hkl*) is needed.] the available models

with meaningful radii parameterization and orientation of the geometric object according to the symmetry. However, symmetry breaking cases can also be treated but require a transformation of the crystal structure to the triclinic space group *P1* (see Ectors *et al.*, 2015a for details) since the multiplicities of respective *hkl* will be broken.

A symmetry following choice can easily be derived from basic crystallographic knowledge. An elegant way is however to use the so-called *normal\_plot* option of *TOPAS* Version 5+ to visualize the refined or modeled morphology directly in order to judge if physical sound parameterization and orientation is present. For this purpose, the three considered geometric models have to be expressed mathematically in spherical coordinates. What seems an easy task is not as obvious as one might think for cylinders and cuboids. Derived from the so-called “superformula” (Gielis, 2003) in two dimensions and “superellipsoids” (e.g., Barr, 1981) in three dimensions two adequate approximations were derived for the model radius in dependence of  $\theta$  and  $\varphi$  as:

For an elliptic cylinder with the radii  $r_x$ ,  $r_y$ , and  $r_z$ :

$$r(\theta, \varphi) = [|r_z^{-1} \cos \varphi|^{10} + |\sin \varphi|^{10} (|r_y^{-1} \sin \theta|^2 + |r_x^{-1} \cos \theta|^2)^5]^{-\frac{1}{10}} \quad (1)$$

and for a cuboid, respectively:

$$r(\theta, \varphi) = [|r_z^{-1} \cos \varphi|^{10} + |\sin \varphi|^{10} (|r_y^{-1} \sin \theta|^{10} + |r_x^{-1} \cos \theta|^{10})]^{-\frac{1}{10}} \quad (2)$$

These formulas can be “tuned” to even better representations (of the edges) of the geometric models by multiplying the magnitude of the exponents, but because of possible numerical overflows the described equations are sufficient approximations for displaying purposes.

For displaying the ellipsoid, the fact that  $\varepsilon_K$  of a triaxial ellipsoid-shaped crystallite is just another smaller ellipsoid is exploited in the following macro. For completeness a similar equation for a triaxial ellipsoid is:

$$r(\theta, \varphi) = [|r_z^{-1} \cos \varphi|^2 + |\sin \varphi|^2 (|r_y^{-1} \sin \theta|^2 + |r_x^{-1} \cos \theta|^2)]^{-\frac{1}{2}} \quad (3)$$

The additional new macro for directly displaying the refined geometric model *PlotAnisoCS* for *TOPAS* reads:

```
macro PlotAnisoCS
{
'ellipsoid
normals_plot = If(modx < 2, sizeL*(3/4),
'cylinder
If(modx < 3,
1/((((Abs((1/cx)*cosphirot))^10)+((Abs((sinphirot))^10))*
(((Abs((1/bx)*sintheta)^2) + ((Abs((1/ax)*costhetarot))^
(2)))^5))^1/10)),
'cuboid
1/((((Abs((1/cx)*cosphirot))^10)+((Abs((sinphirot))^10))*
(((Abs((1/bx)*sintheta)^10) + ((Abs((1/ax)*costhetarot))^
^10))))^1/10)
);}
```

Alongside with the Gaussian component (*AnisoCSg*) which is important for the derivation of respective size distributions a typical call of the macros for example for the refinement of a biaxial cylinder in a trigonal/hexagonal system would look like:

```
str
...
AnisoCS(2, 0, 0, 1, 1, 0, 0, rx, 5, rx, 5, rz, 10, !pc, 0, !tc, 0, !nc,
0, 0)
AnisoCSg(tau, 1)
AnisoCSgout(result.txt)
PlotAnisoCS
```

It is now indeed very simple to identify symmetry breaking parameterization of the geometric model and/or orientation as shown in Figure 2. Only proper parameterization and orientation will display the expected geometric model and thus will lead to sound results.

Clearly the *normals\_plot* feature of *TOPAS V5+* is not only a visual benefit, but also a very educative tool since additionally the plotting feature is aware of orientation thus displays the orthogonal geometric model in reference to the real-space lattice vectors (be aware that the orientation vectors *Z* and *X* are always chosen in reference to the reciprocal lattice vectors). Note also that the *normals\_plot* option produces only normalized morphologies.

#### IV. SAMPLE CASE

In order to demonstrate the benefit of a routine treatment of pronounced anisotropic size peak broadening a commercially acquired hydrated lime sample was measured on a laboratory scale diffractometer and analyzed assuming an isotropic size model and a cylinder model for the portlandite phase. Effectively only one additional refinement parameter was introduced in reference to the isotropic refinement

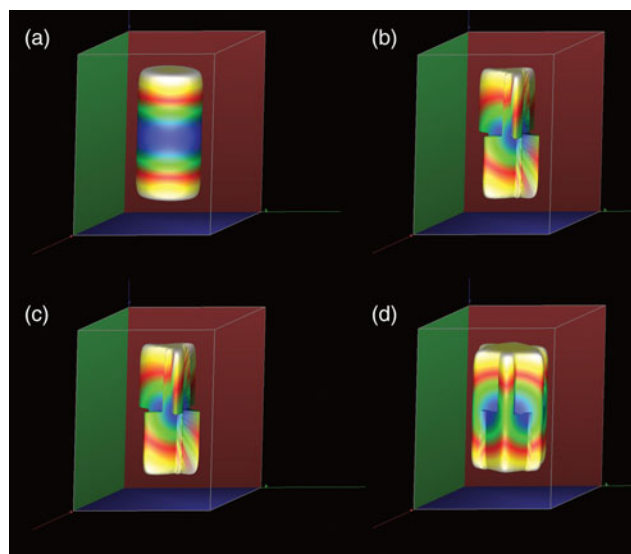


Figure 2. (Color online) (a) A properly oriented and parameterized cylinder in a trigonal crystal system. (b) The same cylinder with a wrong (non-orthogonal) *X* vector choice. (c) Attempt to fit an elliptic cylinder model in a trigonal crystal system. (d) Attempt to fit a cuboid model in a trigonal crystal system.

resulting in a severe drop of the  $R_{wp}$  factor and a clear improvement of the fit quality as can be observed in Figure 3.

Portlandite being a typical layered structure normal to  $c^*$  is often observed to crystallize in pseudo-hexagonal platy prisms which is in good agreement with the displayed morphology. The refined microstructure parameters indicate a negligible strain (“maximum strain”  $e_0$  of 0.072%) and respective area (or surface)-weighted cylinder diameter in the  $(hk0)$  direction of 46.9 nm and height in  $(00l)$  of 9.6 nm with volume-weighted counterparts corresponding to 76.0 and 15.6 nm, respectively. The high ratio (1.62) between the volume- and area-weighted values indicate a rather broad size distribution. These values and the resulting morphology should without further evidence always be interpreted as effective values and morphology, since it cannot be claimed that the proportions of the aspect ratio is necessarily a constant in real samples. Technically one would have to consider a distribution of diameters and heights separately still with the assumption that the orientation and shape is invariant.

This sample demonstrates how the addition of only one additional physical sound size parameter efficiently can improve the fit dramatically as indicated by the reduction of the  $R_{wp}$  from 7.16 to 4.78% and the  $R_{Bragg}$  of the used (room temperature) portlandite structure [space group  $P\bar{3}m1$ , refined lattice parameters  $a$  3.5895(1) and  $c$  4.9108(1) Å, from Henderson and Gutowsky, 1962] from 2.26 to 0.86%.

For completeness the two used initial macro calls:

Isotropic:

```
str
...
AnisoCS(1, 0, 0, 1, 1, 0, 0, rx, 5, rx, 5, rx, 5, !pc, 0,
!tc, 0, !nc, 0, 0)
AnisoCSg(tau, 1)
PlotAnisoCS
```

For the anisotropic cylinder model:

```
str
...
AnisoCS(2, 0, 0, 1, 1, 0, 0, rx, 5, rx, 5, rz, 5, !pc, 0,
!tc, 0, !nc, 0, 0)
AnisoCSg(tau, 1)
PlotAnisoCS
```

#### V. ACCURACY

In this paragraph, the accuracy of the developed model to physical line profiles is evaluated by fitting simulated data by means of the *WPPM* approach as realized in the *PM2K* (Leoni *et al.*, 2006) software. In order to evaluate the accuracy of the Voigt approximation to the line profile using an isotropic case under common laboratory conditions three different log-normal distributions widths, from narrow to broad, with three individual size ranges were simulated in a cubic crystal system with a step size of  $0.01^\circ 2\theta$   $\text{CuK}\alpha$  using the *PM2K* software. Evaluation was done using *TOPAS* Version 5 with an appropriated so-called *hkl* phase. The profile calculation and weighting options of *TOPAS* were kept to the default setting. The refined parameters in this case were the respective radii  $r_x$  for a spherical model, the distribution parameter  $\tau$  and individual scale factors for the individual peaks. A total of nine simulated distributions were evaluated with area-weighted sphere diameters of 10, 50,



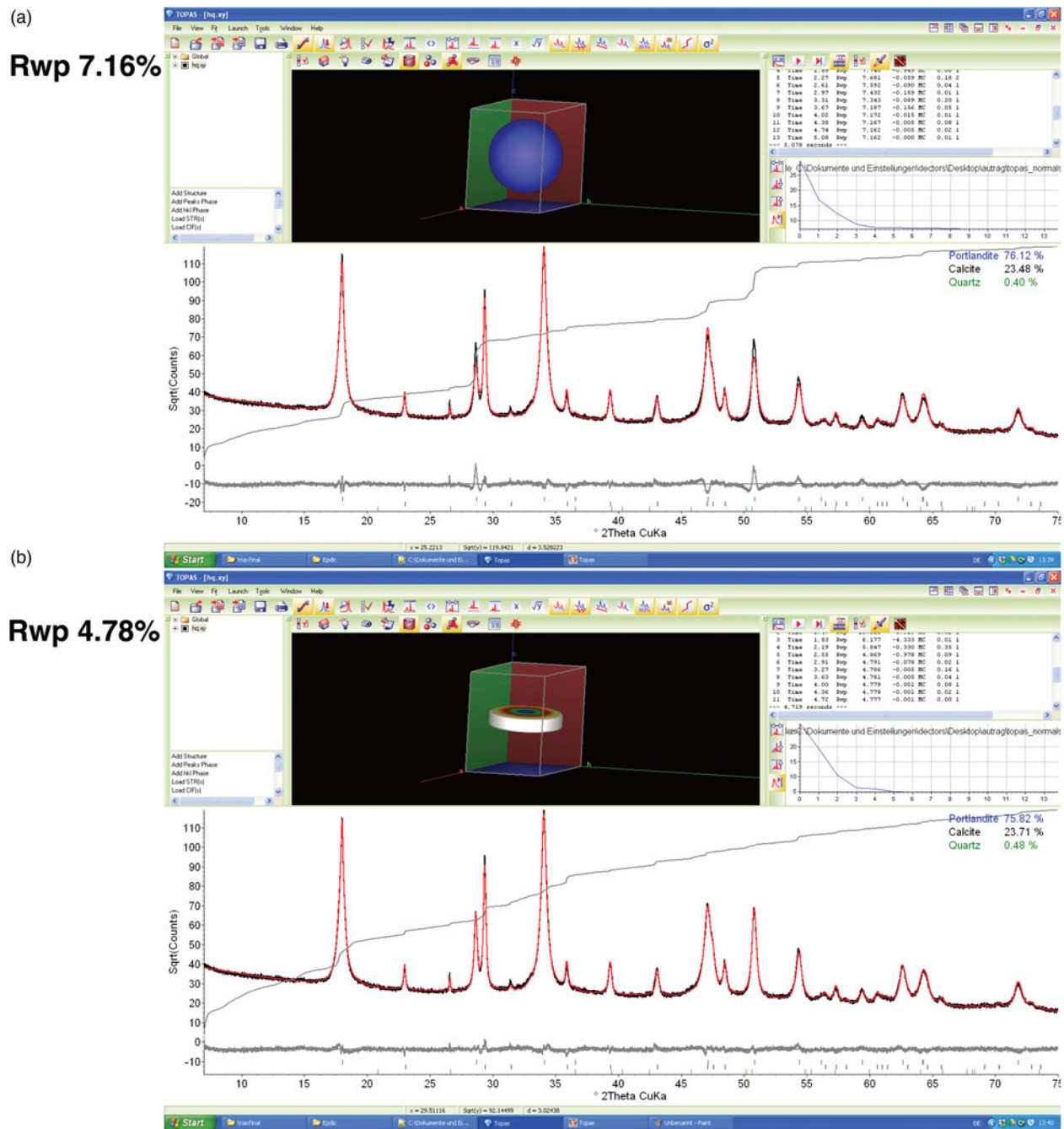


Figure 3. (Color online) (a) Refinement of the hydrated lime sample with an isotropic crystallite size model. Severe misfits are visible for the  $(010/012/110)$  peaks of portlandite at approximately  $(28.7/47.1/50.8^\circ 2\theta)$ . Notably a Pawley-refinement does not solve the misfits. (b) Refinement of the hydrated lime sample with the cylinder crystallite size model. A biaxial ellipsoid model was also tested but resulted in a slightly higher  $R_{wp}$  value of 4.94%.  $R_{exp}$  is 3.09% for both refinements.

and 100 nm and corresponding volume-weighted counterparts of 1.1 (called narrow), 1.3 (called medium), and 1.5 (called broad) times the area-weighted diameters, respectively. The reason to choose those two variation parameters is on the one hand that approaching the 100 nm region the Bragg peaks get very narrow frequently cited as being the limiting “size” for reasonable evaluation. On the other hand, with the lognormal distributions getting very broad the respective Gaussian contribution dramatically decreases, leading to so-called super-Lorentzian peak shapes (Balzar and Ledbetter, 1993). Such behavior is not observed with the other frequently assumed  $\gamma$  distributions (Popa and Balzar, 2002).

In general, we expect the size evaluation to be reasonable if the deviation from the simulated value is within approximately 10% relative. Figure 4 displays the results of the derived area- and volume-weighted sphere diameters. The error bars indicate the 10% error range from the simulated values.

It can be clearly observed from Figure 4 that all refined sizes are very reasonably in the range of the simulated values. Only the results from broad distributions are slightly outside the 10% criterion. The highest deviation (13.5%) in the area-weighted diameters is a refined 8.7 nm in respect to the simulated 10.0 nm. The highest deviation (9.4%) in the volume-weighted diameter being a refined 135.8 nm in respect

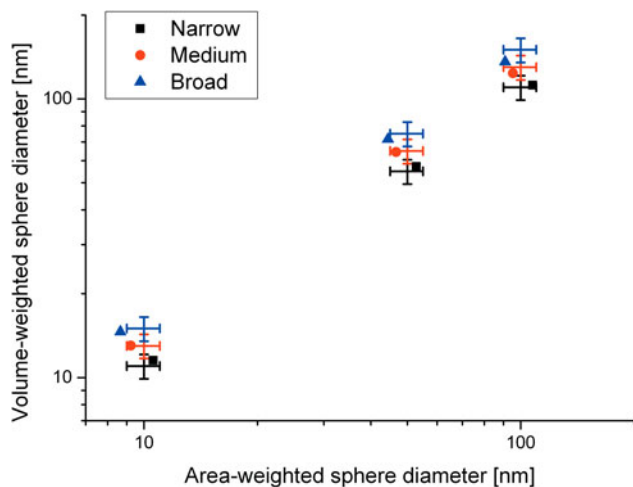


Figure 4. (Color online) Results of the fitting of the *AnisoCS* and *AnisoCSg* macros to simulated sphere distributions from the *WPPM* method. Error bars indicate the 10% relative error range from the simulated values.

to the simulated value of 150.0 nm. In awareness of the approximation of the physical line profile by a Voigt function, the results can be considered very reasonable.

Of course, more interesting in the scope of this paper is the accuracy when considering anisotropic crystallite sizes, since the former results also can be obtained using the implemented procedures in *TOPAS* or with the double-Voigt approximation, still it is of course of importance to be aware of the range of approximation of the double-Voigt approach.

In order to evaluate the accuracy of anisotropic cases, including size distributions two sets of cylinders in a trigonal/hexagonal crystal system were again simulated using the *WPPM* approach as realized in *PM2K*. In this case, lognormal distributions were chosen to reflect a ratio of 1.2 for the volume-weighted to area-weighted cylinder diameters and heights. The cylinder height (*00l*) to diameter (*hk0*) ratio was varied from 0.25 up to 4. The two size ranges were evaluated, namely with area-weighted cylinder diameters of 10 nm (referred to as the 10 nm series) and 50 nm (referred to as the 50 nm series). The fitting results are visualized in Figure 5.

Clearly the results of Figure 5 demonstrate that the refinement method for anisotropic crystallites is in good agreement with the simulated line profiles. The largest discrepancy in the height on diameter is observed at the cylinder distributions with area-weighted diameters of 50 nm with a corresponding cylinder height of 200 nm (cylinder height on diameter 4). This demonstrates that the practical limit for reasonable size evaluation is as often cited in the range of 100–200 nm.

## VI. ACCURACY IN PRESENCE OF ISOTROPIC STRAIN

So far, microstrain-free simulations have been evaluated. The practical difficulty is however often the deconvolution of size and strain effects. The double-Voigt approach is perfectly suitable for such deconvolution without further analysis procedures required. In order to evaluate again in a practical way the efficiency of the later approach the already considered distributions of cylinders were resimulated with the inclusion of isotropic microstrain. For that purpose one can understand isotropic microstrain as a distribution of lattice parameters. The simulated isotropic strain contribution was therefore

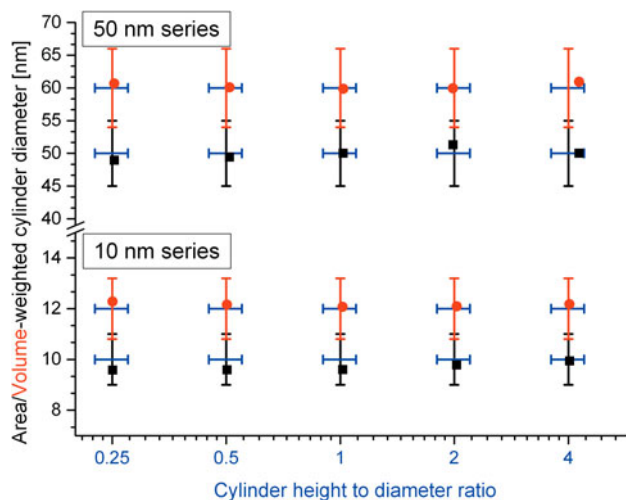


Figure 5. (Color online) Results of the fitting of the *AnisoCS* and *AnisoCSg* macros to simulated cylinder distributions with different height-to-diameter ratios from the *WPPM* method. Error bars indicate the 10% relative error range from the simulated values. Black squares and red dots represent the attained area- and volume-weighted cylinder diameters, respectively. The height-to-diameter ratio on the *x*-scale is constant for both area- and volume-weighted cylinder diameters (*x*-scale in  $\log_2$  scaling for display purposes).

achieved by inclusion of a discrete symmetric triangular-like function to the relative *d*-values as visualized in Figure 6. The corresponding maximum deviation from the reference lattice parameters is  $\pm 0.7\%$  relative.

In Figure 7, the corresponding refined results with a refined strain contribution (Gaussian & Lorentzian strain contributions freely refined) are visualized.

While the results of 10 nm series display good agreement the 50 nm series displays still acceptable results, only with the very high cylinder height (200 nm) showing a deviation outside the defined criterion. This can be very well understood since in the 10 nm series the size effect on the peak broadening is dominating; however, in the 50 nm series the microstrain broadening is a very dominant effect as shown in Figure 8.

When neglecting the cylinder distribution with area-weighted diameters of 50 nm with a corresponding cylinder

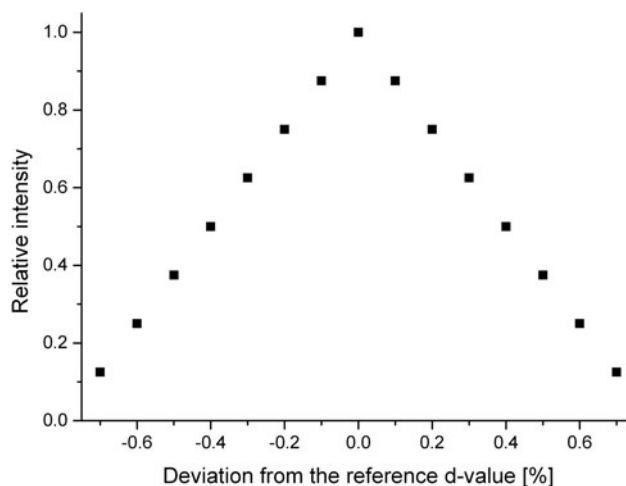


Figure 6. The used *d*-value dispersion distribution in order to simulate an isotropic strain contribution.

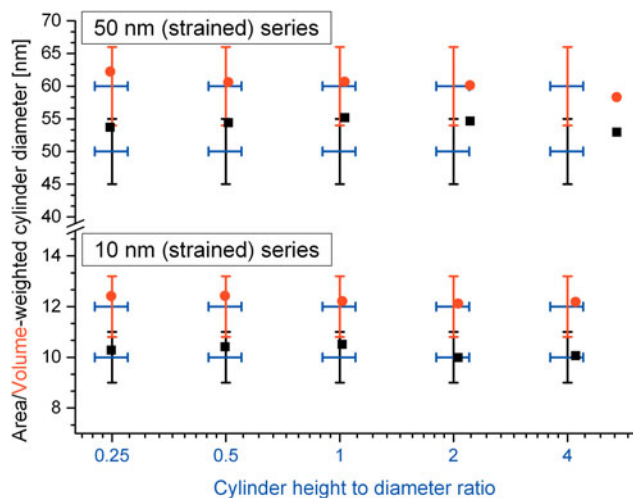


Figure 7. (Color online) Results of the fitting of the *AnisoCS* and *AnisoCSg* macros to simulated cylinder distributions with different height-to-diameter ratios and isotropic microstrain from the *WPPM* method. Error bars indicate the 10% relative error range from the simulated values. Black squares and red dots represent the attained area- and volume-weighted cylinder diameters, respectively. The height-to-diameter ratio on the  $x$ -scale is constant for both area- and volume-weighted cylinder diameters ( $x$ -scale in  $\log_2$  scaling for display purposes).

height of 200 nm the results fit very well in the defined 10% margin. The average derived “maximum strain”  $\epsilon_0$  of the 10 nm series is 0.19(1)% and for the 50 nm series 0.20(2)%, which is in reasonable agreement of the expected value from the simulation of 0.1875% in the  $\epsilon_{0(\text{FWHM})}$  definition used by the *TOPAS* software.

When erroneously no strain is considered very visible misfits were observed. Inclusion of the strain refinement, e. g. of the 10 nm series lead to a drop of the  $R_{\text{wp}}$  in the range of 43–88% relative.

The deconvolution of isotropic microstrain in the double-Voigt approach critically depends on the presence of at least one well-resolved second-order reflection. Fits without second-order reflection in the 10 nm series produced maximum deviations of 43.2, 31.4, and 40.2% for the area-weighted diameters, volume-weighted diameters, and cylinder

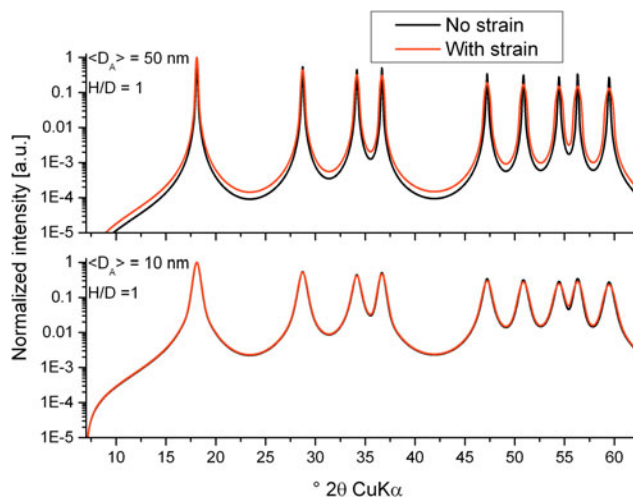


Figure 8. (Color online) Comparison of selected simulated diffraction pattern of the 10 and 50 nm series displaying the effect of the isotropic strain contribution. Note that the 10 nm series with and without strain contribution is almost superimposed.

height on width, respectively. Inclusion of only one second-order reflection reduced the maximum deviations down to very reasonable 9.8, 4.0, and 5.6%, respectively. This demonstrates the absolute need of an appropriate angular  $2\theta$  measurement range for meaningful microstructure analysis in general.

## VII. LIMITATIONS OR A WORD OF WARNING

In microstructure analysis from powder diffraction methods, the degree of information available is always limited and depends on the degree of approximation one is willing to accept. The assumption that the line profile produced from the size effect is a Voigt function of course does not hold. It is a reasonable approximation in most practical cases but will never be able to produce accurate results in all theoretical cases. As far as the double-Voigt approximation is concerned size and morphology effects can be treated with the proposed model on a physical sound basis and even in the case of isotropic strain deconvolution is reasonably successful. Yet, a physical account for “anisotropic” strain contribution as introduced e.g. by dislocations or non-uniform lattice parameter deviations is at the moment not realized to the author’s knowledge in a usable way in the double-Voigt approach though it may, as far as the line profile approximation methods allow, be the model of choice.

Even within the 10% relative error scale derived size distributions can vary very noticeably if a certain distribution function is postulated since the “measurable” area- and volume-weighted parameters are ratios of the higher moments of the distribution. Therefore slight differences in derived distributions should always receive very careful consideration and in the best case should be validated against other microstructure analysis methods or transmission electron microscopy.

The intention of the demonstrated model for anisotropic size treatment is to account in a physically sound, parameter efficient, fast and stable way the considered effects in routine Rietveld refinements.

## VIII. CONCLUSION

We have demonstrated the application of the treatment of anisotropic crystallite sizes with considerations of size distributions and isotropic microstrain in the double-Voigt approach. Within the area-weighted range of 10–100 nm the refined results are very well within an approximated 10% relative error from the simulated values by means of the *WPPM* method. In conclusion, this demonstrates that the deviation of microstructure parameters from common routine laboratory scale Rietveld refinements can provide meaningful physically founded results in the double-Voigt approach. In practice using laboratory scale measurements one can expect the derived value to be at least within 10–20% relative error from the “true” values with the proposed method if the requirements of the data quality, not too broad uniform size distributions and limiting sizes are met by the chosen experimental measurement parameters and the sample under consideration. Even better accuracy is expected with high-resolution diffraction instruments, for instance at synchrotron beamlines, with adequate instrument functions. We sincerely hope that this article serves as a motivation to report meaningful microstructure parameters even in routine application of Rietveld refinements in a sensitive way. Crystallite morphology, the



size and distributions thereof are a valuable source of information, almost exclusively attainable by powder diffraction, often overlooked or treated in an inadequate way in routine evaluations. The learning curve of the meaningful refinement of anisotropic size effects is certainly greatly decreased with the proposed macros and visual feedback using the normals\_plot functionality of the *TOPAS* framework.

## CONFLICTS OF INTERESTS

The authors declare no affiliation with Bruker AXS Inc. or any financial interest in promoting the *TOPAS* software. The authors wish to encourage programmers to implement the demonstrated anisotropic size treatment methodology in a physical sensitive way in Rietveld software for the benefit of more accurate and reliable size parameters.

- Balić Žunić, T. and Dohrup, J. (1999). "Use of an ellipsoid model for the determination of average crystallite shape and size in polycrystalline samples," *Powder Diffr.* **14**(3), 203–207.
- Balzar, D. and Ledbetter, H. (1993). "Voigt-function modeling in Fourier analysis of size- and strain-broadened X-ray diffraction peaks," *J. Appl. Crystallogr.* **26**, 97–103.
- Barr, A. H. (1981). "Superquadrics and angle-preserving transformations," *IEEE Comput. Graph.* **1**(1), 11–23.
- Bertaut, E. (1949a). "Signification de la dimension cristalline mesurée d'après la largeur de raie Debye-Scherrer," *C. R. Acad. Sci.* **228**, 187–189.
- Bertaut, E. (1949b). "Étude aux rayons X de la répartition des dimensions des cristallites dans une poudre cristalline," *C. R. Acad. Sci.* **228**, 492–494.
- Cheary, R. and Coelho, A. (1992). "A fundamental parameters approach to X-ray line-profile fitting," *J. Appl. Crystallogr.* **25**, 109–121.
- Ectors, D. (2016). *Advances in the analysis of cementitious reactions and hydrate phases* (PhD thesis). University of Erlangen-Nuernberg (FAU), available online at: <https://opus4.kobv.de/opus4-fau/frontdoor/index/index/docId/7174>
- Ectors, D., Goetz-Neunhoeffler, F., and Neubauer, J. (2015a). "A generalized geometric approach to anisotropic peak broadening due to domain morphology," *J. Appl. Crystallogr.* **48**, 189–194.
- Ectors, D., Goetz-Neunhoeffler, F., and Neubauer, J. (2015b). "Domain size anisotropy in the double-Voigt approach: an extended model," *J. Appl. Crystallogr.* **48**, 1998–2001. DOI: 10.1107/S1600576715018488/
- Gielis, J. (2003). "A generic geometric transformation that unifies a wide range of natural and abstract shapes," *Am. J. Bot.* **90**(3), 333–338.
- Henderson, D. M. and Gutowsky, H. S. (1962). "A nuclear magnetic resonance determination of the hydrogen positions in  $\text{Ca}(\text{OH})_2$ ," *Am. Mineral.* **47**, 1231–1251.
- Hurle, K., Neubauer, J., and Goetz-Neunhoeffler, F. (2016). "Influence of  $\text{Sr}^{2+}$  on calcium-deficient hydroxyapatite formation kinetics and morphology in partially amorphized  $\alpha$ -TCP," *J. Am. Ceram. Soc.* **99**(3), 1055–1063.
- Langford, J. I. (1980). "Accuracy of crystallite size and strain determined from the integral breadth of powder diffraction lines," *Natl. Bur. Stand. Spec. Publ.* **567**, 255–269.
- Langford, J. I. and Wilson, A. J. C. (1978). "Scherrer after sixty years: a survey and some new results in the determination of crystallite size," *J. Appl. Crystallogr.* **11**, 102–113.
- Langford, J. I., Louër, D., and Scardi, P. (2000). "Effect of a crystallite size distribution on X-ray diffraction line profiles and whole-powder-pattern fitting," *J. Appl. Crystallogr.* **33**, 964–974.
- Leonardi, A., Leoni, M., Siboni, S., and Scardi, P. (2012). "Common volume functions and diffraction line profiles of polyhedral domains," *J. Appl. Crystallogr.* **45**, 1162–1172.
- Leoni, M., Confente, T., and Scardi, P. (2006). "PM2K: a flexible program implementing Whole Powder Pattern Modelling," *Z. Kristallogr. Suppl.* **23**, 249–254.
- Popa, N. C. and Balzar, D. (2002). "An analytical approximation for a size-broadened profile given by the lognormal and gamma distributions," *J. Appl. Crystallogr.* **35**, 338–346.
- Scardi, P. (2008). "Recent advances in whole powder pattern modelling," *Z. Kristallogr. Suppl.* **27**, 101–111.
- Scardi, P. and Leoni, M. (2002). "Whole powder pattern modelling," *Acta Crystallogr.* **A58**, 190–200.
- Scherrer, P. (1918). "Bestimmung der Größe und der inneren Struktur von Kolloidteilchen mittels Röntgenstrahlen," *Nachr. Göttinger Ges.* **1918**, 98–100.
- Stephens, P. W. (1999). "Phenomenological model of anisotropic peak broadening in powder diffraction," *J. Appl. Crystallogr.* **32**, 281–289.
- Stokes, A. R. (1948). "A numerical Fourier-analysis method for the correction of widths and shapes of lines on X-ray powder photographs," *Proc. Phys. Soc. Lond.* **61**(4), 382–391.
- Tournaire, M. (1956a). "Utilisation du deuxième moment comme critère d'élargissement des raies Debye Scherrer. Elimination de l'effet instrumental," *C. R. Acad. Sci.* **242**, 2016–2018.
- Tournaire, M. (1956b). "Utilisation du deuxième moment comme critère d'élargissement des raies Debye Scherrer. Signification physique," *C. R. Acad. Sci.* **242**, 2161–2164.
- von Laue, M. (1936). "Die äußere Form der Kristalle in ihrem Einfluß auf die Interferenzerscheinungen an Raumgittern," *Ann. Phys. (Leipzig)* **26**, 55–68.
- Wilson, A. J. C. (1962a). "Variance as a measure of line broadening," *Nature* **193**, 568–569.
- Wilson, A. J. C. (1962b). *Chapter IV: Powder Patterns of Small Crystals in: X-Ray Optics* (Methuen, London), 2nd ed.